A Novel Adaptive Current Harmonic Detection Method Applied in Multifunctional Single−Phase Solar Inverters

Lucas S. Xavier
Gerência de Especialistas em Sistemas Elétricos de Potência
Universidade Federal de Viçosa
Av. P. H. Rolfs s/n, 36570-000
Viçosa, Brazil
Email: lsantx@gmail.com

Allan F. Cupertino
Centro Federal de Educação Tecnológica de Minas Gerais
Av. Amazonas 5253, 30421-169
Belo Horizonte, Brazil
Email: allan.cupertino@yahoo.com.br

Heverton A. Pereira
Gerência de Especialistas em Sistemas Elétricos de Potência
Universidade Federal de Viçosa
Av. P. H. Rolfs s/n, 36570-000
Viçosa, Brazil
Email: heverton.pereira@ufv.br

***Abstract*—The inverter multifunctional operation is an interesting concept to improve the power quality index of an installation. This approach is based on the harmonic current compensation, generated by nonlinear loads. An important issue for the multifunctional operation is the harmonic detection method. The traditional methods detects all harmonic contents of the load current and the control tuning tends to be complex and few flexible, once the load harmonic contents are not well defined. Therefore, this work proposes a novel adaptive current harmonic detection method applied in multifunctional single-phase photovoltaic inverters. The proposed strategy is frequency adaptive and able to detect the load harmonic current with higher amplitude. This method consists in a cascade association of two phase-locked loop based on second order generalized integrator (SOGI-PLL). Simulation results show performance of the current harmonic detection method proposed, improving significantly the grid current quality just compensating the higher harmonic contents.**

I. Introduction

The photovoltaic (PV) plants have experienced a high expansion in the worldwide electrical systems in the last years [1]. For this reason, special attention has been paid by researchers in relation to reliability and efficiency of grid-connected photovoltaic systems [2]. The important element in PV systems are the solar inverters. These elements are responsible to extract the maximum power from photovoltaic plant and inject it into the grid [3]. Furthermore, due to variations in solar irradiance, the PV inverters have potential to improve the power quality index at the point of common coupling (PCC) [3], [4], [5], [6].

An interesting mode to improving the power quality index of an installation by means of PV system is aggregating to the inverter control strategy ancillary services, such as, current harmonic compensation. It transforms the inverter in a multifunctional device [3], [6].

In multifunctional operation, the current harmonic detection method is an important issue. However, most proposed methods are not capable to detect the predominant harmonic component frequency [7], [8], [9], [10], [11]. This strategy can be interesting in order to compensate only the current harmonic component with higher amplitude. Thereby, the current controller can be tuned for specific harmonics, increasing efficiency and reducing the control algorithm complexity. The issue on harmonic selectivity has been approached in some works in the literature [12], [13].

In single-phase applications, many works use proportional-resonant (PR) control [14], [15] because the current loop references are sinusoidal. However, PR controller can compensate only one frequency. Therefore, one resonant controller needs to be designed for each harmonic frequency [15]. This fact increases the control algorithm complexity. When the current harmonic contents of a load are not well defined, the proportional-integral (PI) controllers can be an interesting solution. However, with many harmonic orders, the PI controller has steady state error due to its limited current tracking capability.

In this context, this work proposes a novel adaptive current harmonic detection method applied in a single-phase multifunctional inverter able to detect the load current harmonic component with higher amplitude. This detection method consists in a cascade association of two phase-locked loop based on a second order generalized integrator (SOGI-PLL) proposed in [16].

This proposed detection method is based on the adaptive characteristic of the second order generalized integrator (SOGI) [16], [17]. The SOGI can be tuned by feedback of the detected frequency. Some works use the SOGI feedback to make it adaptive under distorted grid conditions [9], [18].

The novel detection method is applied in a single-phase PV system as shown in Fig. 1. The control system is based on a linear PI control. Electrical model of the solar panel proposed in [19] is used. An algorithm of maximum power point tracking (MPPT) calculates the reference of dc-bus voltage.

978-1-4673-6605-2/15/$31.00 ©2015 IEEE

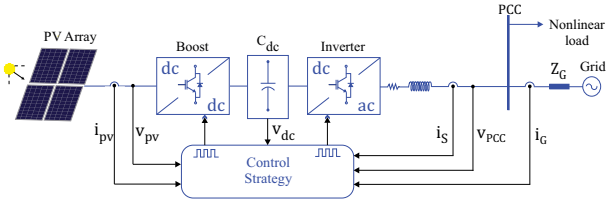

Fig. 1. Grid-connected photovoltaic system based on multifunctional inverter.

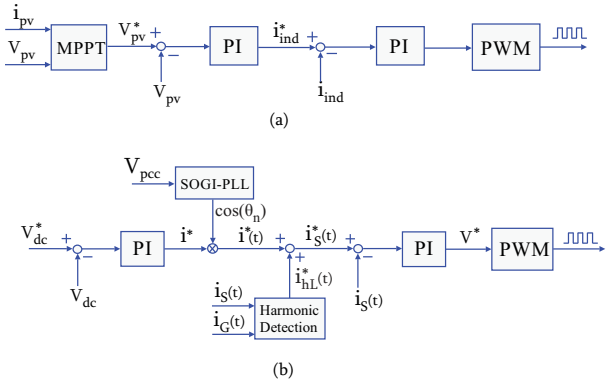

Fig. 2. Complete control strategy. (a) Boost control strategy. (b) Inverter control strategy.

II. Control Strategy

Complete control strategy is presented in Fig. 2. The MPPT, used in the dc/dc boost converter control loop, maintains the solar array delivering maximum power to the system at various levels of solar irradiance and temperature. Operating principle of this algorithm used is based on perturbation and observation (P&O) method [20]. The dc/dc stage uses a current mode control structure, which is detailed in Fig. 2(a).

Inverter control strategy is shown in Fig. 2(b). The PI compensator is used in the dc-bus voltage control. This compensator calculates the active current amplitude i^*, which needs to be injected into the power system. This signal is synchronized with PCC voltage through SOGI-PLL structure [16], [17], resulting in a sinusoidal waveform $i^*(t)$. This current reference is added to load harmonic component detected, generating the current reference $i^*_S(t)$. Finally, $i^*_S(t)$ is compared with the inverter current. Another PI compensator calculates the converter modulation index V^*.

Generally, loads in an installation are connected in different points and the direct measurement of its current can be difficult. This work estimates the load current in terms of inverter injected current and grid current, to ensure the harmonic compensation of all loads connected to the PCC.

III. Adaptive Current Harmonic Detection Method

In order to compensate just one load harmonic current component in an installation, this work proposes a detection method able to detect the load harmonic current component with higher amplitude.

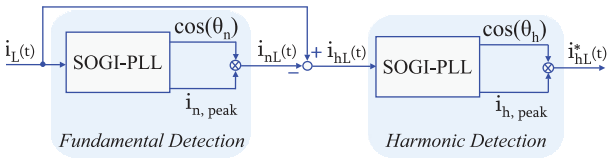

Fig. 3. Current harmonic detection proposed based on SOGI-PLL.

The detection strategy is based on cascaded association of two phase-locked loops (PLL) based on second order generalized integrator (SOGI), as shown in Fig. 3. The detailed description about these structures are shown in [16], [17], [21], [22].

The first stage consists to detect the load fundamental current component $i_{nL}(t)$. In steady state, the measured load current $i_L(t)$ is filtered by SOGI tuned in the fundamental frequency, detected by the PLL. This is done making $i_q = 0$. The complete SOGI-PLL structure for fundamental component detection is shown in Fig. 4. As depicted in [16], the closed-loop transfer functions of the SOGI are defined as:

$$H_d(s) = \frac{i_L^{'}}{i_L}(s) = \frac{k\omega s}{s^2 + k\omega s + \omega^2} \quad (1)$$

$$H_q(s) = \frac{qi_L^{'}}{i_L}(s) = \frac{k\omega^2}{s^2 + k\omega s + \omega^2} \quad (2)$$

where ω is the resonant frequency and k is a damping factor, which is responsible for SOGI's bandwidth, as detailed in the bode diagrams shown in Fig. 5 and Fig. 6. It is observed in this structure a bandpass filter characteristic, with adjustable resonant frequency ω.

In the fundamental component detection, the SOGI gain is set to $k = \sqrt{2}$ which results in an optimal relationship between the settling time and suppression of unwanted frequencies [17]. However, the current may have a high harmonic contents. For this reason, the low order harmonics close to the fundamental frequency can impact the SOGI-PLL performance. Therefore, the PLL bandwidth is reduced and the low pass filters (LPF) are used in the frequency and amplitude detection to avoid these oscillations, as illustrated in Fig. 4.

The second loop stage consists to detect the harmonic contents with higher amplitude in the load current $i^*_{hL}(t)$. In order to ensure the rotation of the space phasor orthogonal to the q-axis, another PLL should be adjusted to the new signal and to extract the angle and frequency of the harmonic component with higher amplitude of the load current. This frequency is used as feedback to another SOGI and it provides two quadrature signals filtered in this frequency. This process eliminates the harmonics of low amplitude and detects the angle and amplitude of the predominant harmonic. The structure of SOGI-PLL for harmonic component detection stage is similar to Fig. 4.

Current fundamental component $i_{nL}(t)$ is detected by the following multiplication:

$$i_{nL}(t) = i_{n,peak} cos(\theta_n) \quad (3)$$

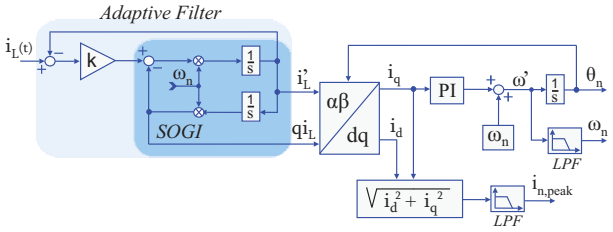

Fig. 4. General structure of a single-phase phase-locked loop (PLL).

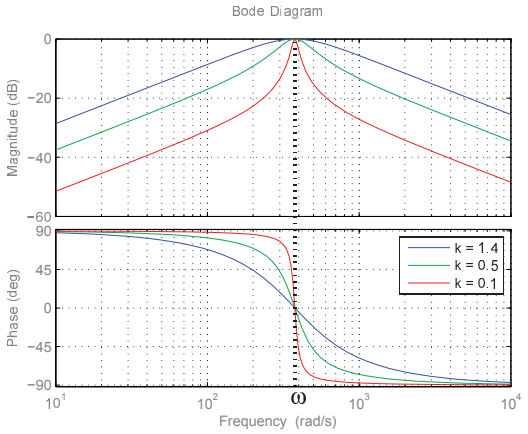

Fig. 5. Bode diagram of H_d.

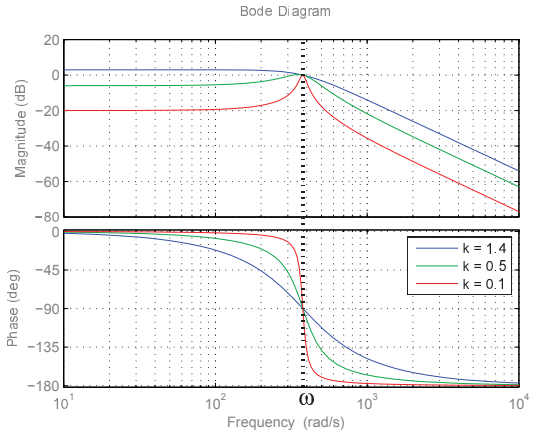

Fig. 6. Bode diagram of H_q.

The PLL used in the harmonic component detection loop has wide bandwidth in order to obtain fast stabilization in the angle and frequency detection. However, the SOGI is set to narrow bandwidth ($k = 0.4$), which results in an optimal suppression of unwanted frequencies.

Furthermore, a LPF is used to support in the suppression the oscillations. Therefore, the harmonic component with higher amplitude in the load current $i^*_{hL}(t)$ is detected by 4. This detected signal is sent to the control strategy for harmonic compensation.

$$i^*_{hL}(t) = i_{h,peak} cos(\theta_h). \quad (4)$$

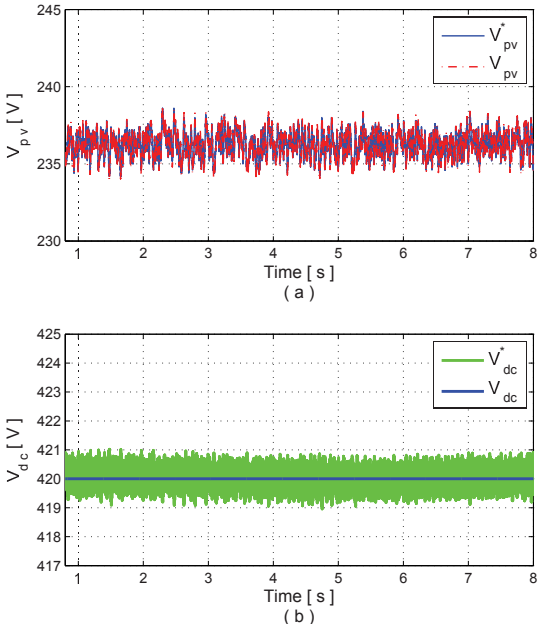

Fig. 7. (a) Voltage at maximum power point of the solar plant. (b) Inverter dc-bus voltage.

IV. Results

The case study presents a solar array with 5 parallel strings of 13 panels of 48 W in series. The inverter rated power is 4kVA , which corresponds to 30% of overload capability. The boost and inverter switching frequency is 12 kHz. Voltage at point of common couple is 220 V. The discrete simulation was implemented in Matlab/Simulink environment with sample time of twice the switch frequency.

The solar irradiance is maintained in 500 W/m^2 during the study. The solar array voltage profile (V_{pv}) is illustrated in Fig. 7(a). This voltage tracks the maximum power point due to MPPT algorithm presents in the boost converter control strategy. The inverter dc-bus voltage (V_{dc}) is controlled in 420 V as detailed in Fig. 7(b).

The nonlinear loads connected to the PCC are represented by current sources, injecting harmonics in the system. In the simulation, the load current harmonic contents are changed to validate the new harmonic detection method proposed. The load current contents during the time intervals are shown in the spectrum in Fig. 8. Between $0 < t < 2$s, the load current harmonic contents has 5th and 7th harmonic with amplitude of 3 A and 1 A, respectively (Fig. 8(a)). Between $2 \leq t < 4$, the load current has a 5th and 7th harmonic of 1 A and 5 A, respectively (Fig. 8(b)). Between $4 \leq t < 6$, the load harmonic contents has a 5th and 7th harmonic, both with amplitude of 2 A (Fig. 8(c)). Between $6 \leq t \leq 8$, the load current has a 3rd, 5th and 7th harmonic with amplitude of 6 A, 2 A and 0.5A, respectively (Fig. 8(d)).

The amplitude of the load fundamental current is maintained at 20 A in both cases. The fundamental component of the detected load current is illustrated in Fig. 9. As the funda-

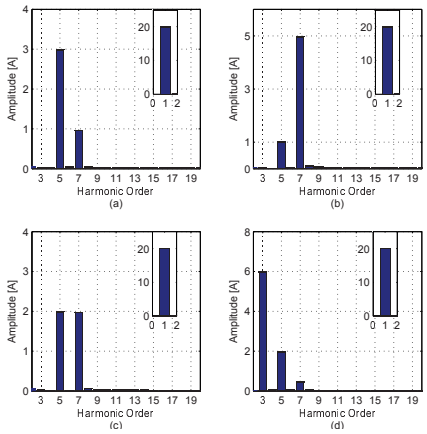

Fig. 8. Load current spectrum, illustrating the changes in the harmonic contents for the validation of the harmonic detection method proposed. (a) Between $0 < t < 2$ seconds. (b) Between $2 \leq t < 4$ seconds. (c) Between $4 \leq t < 6$ seconds. (d) Between $6 \leq t \leq 8$ seconds.

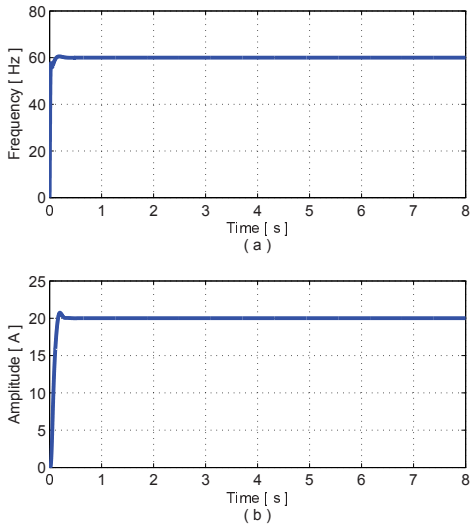

Fig. 9. Fundamental component of the load current detected. (a) Signal frequency. (b) Signal amplitude.

mental component is not changed, the detected frequency and amplitude are constants during the simulation, as shown in Fig. 9(a) and Fig. 9(b), respectively. The detected amplitude and frequency of the load harmonic component with higher amplitude is illustrated in Fig. 11. The harmonic compensation is enabled at 1 second. Initially, the 5th harmonic is detected. Between $2 \leq t \leq 4$ seconds the 7th is detected. Between $4 \leq t < 6$ seconds the 5th and 7th harmonic of the load current have the same amplitude. For this reason, as the detector was already tracking the 7th the detector PLL still locked for the 7th. Between $6 \leq t \leq 8$ seconds the 3rd is detected as harmonic with higher amplitude in the load current contents.

The detected harmonic is reconstructed and used by the current control to perform the harmonic compensation. Details on the detected 7th harmonic and its reconstruction are shown in Fig. 10.

The compensation of the harmonic with higher amplitude in

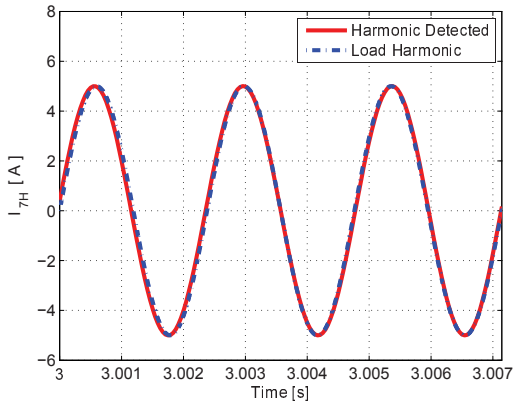

Fig. 10. Details on the 7th harmonic of the load current and details on the signal detected and rebuilt.

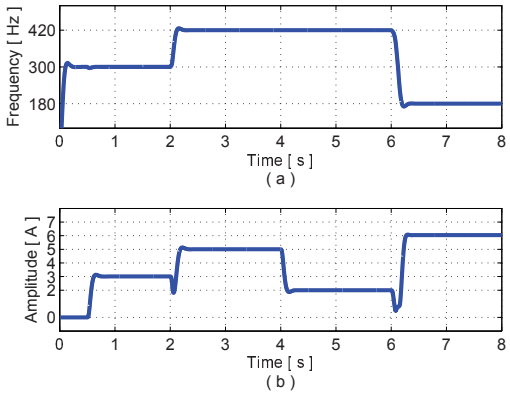

Fig. 11. Harmonic component with higher amplitude detected of the load current. (a) Signal frequency. (b) Signal amplitude.

the load current contents can greatly improve the grid power quality with reduced control algorithm complexity. Details of the grid current (i_G) and inverter current (i_S) when the harmonic compensation is enabled in 1 second are shown in Fig. 12(a) and Fig. 12(b), respectively.

The Fig. 12(c) shows the spectrum of the grid and inverter current during the harmonic compensation between $1 \leq t < 2$ seconds. Note the suppression of the 5th harmonic in the grid current.

Between $2 \leq t < 6$ seconds, the 7th harmonic of the load current is strongly reduced in the grid current, as shown in Fig. 12 and Fig. 13. After 6 seconds, the 3rd harmonic of the load current is compensated, as detailed in Fig. 14.

The Table I details the total harmonic distortion (THD) of the grid, inverter and load current during the harmonic compensation. The Table II details the currents THD for the same simulation without harmonic compensation. Note that, the strongly improvement of the grid power quality index. Between $6 \leq t \leq 8$, e.g., the grid current THD reduces of 54.84 % (Table II) to 19.06 % (Table I).

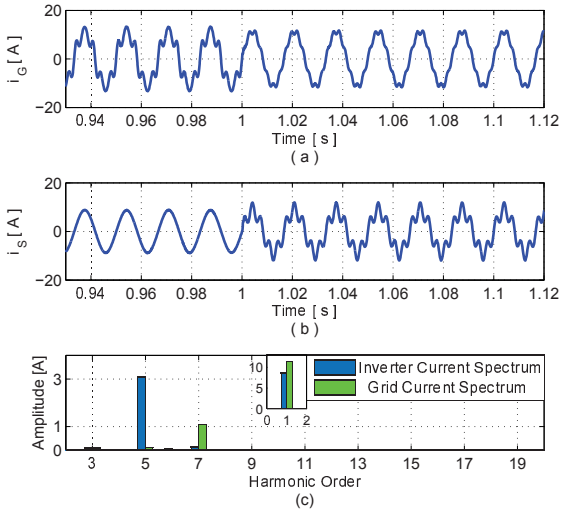

Fig. 12. (a) Grid current detail when the harmonic compensation is enabled in 1 second. (b) Inverter current detail in 1 second. (c) Spectrum of inverter and grid current between $1 \leq t < 2$ seconds.

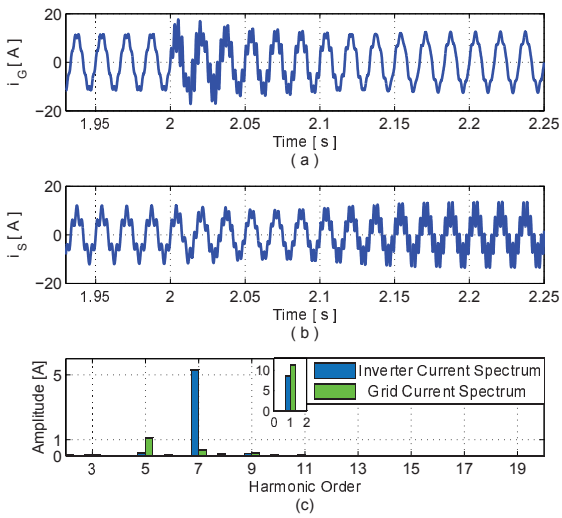

Fig. 13. (a) Grid current detail in 2 seconds. (b) Inverter current detail in 2 seconds. (c) Spectrum of inverter and grid current between $2 \leq t < 4$ seconds.

V. Conclusion

This work presented a novel adaptive current harmonic detection method applied in multifunctional single-phase photovoltaic inverters. This method consists in a cascade association of two phase-locked loop based on second order generalized integrator (SOGI-PLL).

The proposed strategy is frequency adaptive and able to detect the load current harmonic with higher amplitude. Thereby, the current controller can be tuned for specific harmonics, increasing efficiency and reducing the control algorithm complexity.

Simulation results showed the current harmonic detection proposed method performance, which provided partial harmonic compensation.

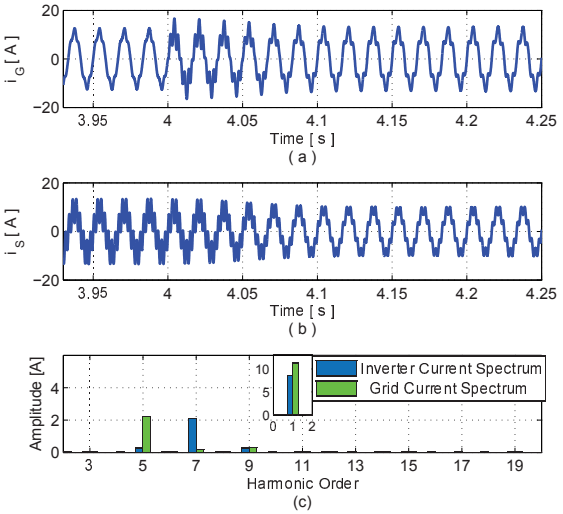

Fig. 14. (a) Grid current detail in 4 seconds. (b) Inverter current detail in 4 seconds. (c) Spectrum of inverter and grid current between $4 \leq t < 6$ seconds.

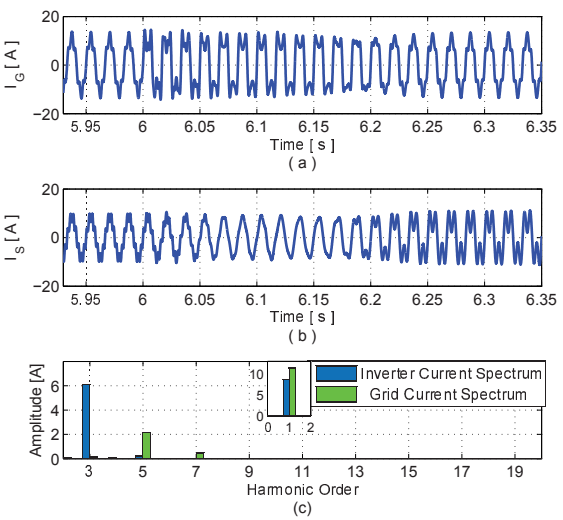

Fig. 15. (a) Grid current detail in 6 seconds. (b) Inverter current detail in 6 seconds. (c) Spectrum of inverter and grid current between $6 \leq t \leq 8$ seconds.

TABLE I
Total Current Harmonic Distortion During Harmonic Compensation

Intervals	THD i_G (%)	THD i_S (%)	THD i_L (%)
$0 < t < 1$	27.83	1.18	15.69
$1 \leq t < 2$	9.9	35.57	15.69
$2 \leq t < 4$	10.72	60.89	25.39
$4 \leq t < 6$	19.73	24.64	14.02
$6 \leq t < 8$	19.06	72.83	31.48

The load connected at the point of common couple of the case study presented 3rd, 5th and 7th harmonic. The harmonic with higher amplitude was compensated and the results suggest improvements in the grid power quality indexes.

TABLE II
TOTAL CURRENT HARMONIC DISTORTION WITHOUT HARMONIC COMPENSATION

Intervals	THD i_G (%)	THD i_S (%)	THD i_L (%)
$0 < t < 1$	27.83	1.18	15.69
$1 \leq t < 2$	28.23	1.20	15.69
$2 \leq t < 4$	45.70	1.17	25.39
$4 \leq t < 6$	24.95	1.15	14.02
$6 \leq t < 8$	54.84	1.30	31.48

ACKNOWLEDGMENT

The authors would like to thank the Brazilian agencies CAPES, FAPEMIG and CNPQ, which supported this work.

REFERENCES

[1] REN21, "Annual reporting on renewables:ten years of excellence," *Renewables 2015 Global Status Report*, 2015.

[2] E. Romero-Cadaval, G. Spagnuolo, L. Garcia Franquelo, C. Ramos-Paja, T. Suntio, and W. Xiao, "Grid-connected photovoltaic generation plants: Components and operation," *Industrial Electronics Magazine, IEEE*, vol. 7, no. 3, pp. 6–20, Sept 2013.

[3] J. Bonaldo and J. Antenor Pomilio, "Multi-functional use of single-phase power converters," in *Innovative Smart Grid Technologies Latin America (ISGT LA), 2013 IEEE PES Conference On*, April 2013.

[4] R. Carnieletto, S. Suryanarayanan, M. Simoes, and F. Farret, "A multifunctional single-phase voltage source inverter in perspective of the smart grid initiative," in *Industry Applications Society Annual Meeting, 2009. IAS 2009. IEEE*, Oct 2009.

[5] S. Rahmani, A. Hamadi, K. Al-Haddad, and H. Kanaan, "A multifunctional power flow controller for photovoltaic generation systems with compliance to power quality standards," in *IECON 2012 - 38th Annual Conference on IEEE Industrial Electronics Society*, Oct 2012.

[6] L. Xavier, A. Cupertino, and H. Pereira, "Adaptive saturation scheme for a multifunctional single-phase photovoltaic inverter," in *Industry Applications (INDUSCON), 2014 11th IEEE/IAS International Conference on*, Dec 2014.

[7] H. Akagi, Y. Kanazawa, and A. Nabae, "Instantaneous reactive power compensators comprising switching devices without energy storage components," *Industry Applications, IEEE Transactions on*, vol. IA-20, no. 3, pp. 625–630, May 1984.

[8] B. McGrath, D. Holmes, and J. Galloway, "Power converter line synchronization using a discrete fourier transform (dft) based on a variable sample rate," *Power Electronics, IEEE Transactions on*, vol. 20, no. 4, pp. 877–884, July 2005.

[9] P. Rodrguez, A. Luna, I. Candela, R. Mujal, R. Teodorescu, and F. Blaabjerg, "Multiresonant frequency-locked loop for grid synchronization of power converters under distorted grid conditions," *Industrial Electronics, IEEE Transactions on*, vol. 58, no. 1, pp. 127–138, Jan 2011.

[10] Y. F. Wang and Y. W. Li, "Three-phase cascaded delayed signal cancellation pll for fast selective harmonic detection," *Industrial Electronics, IEEE Transactions on*, vol. 60, no. 4, pp. 1452–1463, April 2013.

[11] H. Paredes, D. Brandao, T. Terrazas, and F. Marafao, "Shunt active compensation based on the conservative power theory current's decomposition," in *Power Electronics Conference (COBEP), 2011 Brazilian*, Sept 2011.

[12] J. Bonaldo, H. Morales Paredes, and J. Antenor Pomilio, "Control of single-phase power converters connected to low voltage distorted power systems with variable compensation objectives," *Power Electronics, IEEE Transactions on*, vol. PP, no. 99, pp. 1–1, 2015.

[13] Y. Yang, K. Zhou, and F. Blaabjerg, "Frequency adaptability of harmonics controllers for grid-interfaced converters," *International Journal of Control*, vol. 00, no. 0, p. 115, February 2015.

[14] A. Cupertino, L. Carlette, F. Perez, J. Resende, S. Seleme, and H. Pereira, "Use of control based on passivity to mitigate the harmonic distortion level of inverters," in *Innovative Smart Grid Technologies Latin America (ISGT LA), 2013 IEEE PES Conference On*, April 2013.

[15] J. He, Y. W. Li, F. Blaabjerg, and X. Wang, "Active harmonic filtering using current-controlled, grid-connected dg units with closed-loop power control," *Power Electronics, IEEE Transactions on*, vol. 29, no. 2, pp. 642–653, Feb 2014.

[16] M. Ciobotaru, R. Teodorescu, and F. Blaabjerg, "A new single-phase pll structure based on second order generalized integrator," in *Power Electronics Specialists Conference, 2006. PESC '06. 37th IEEE*, June 2006.

[17] R. Teodorescu, M. Liserre, and P. Rodrguez, *Grid Converters for Photovoltaic and Wind Power Systems*. Wiley-IEEE Press, 2011.

[18] P. Rodriguez, A. Luna, I. Candela, R. Teodorescu, and F. Blaabjerg, "Grid synchronization of power converters using multiple second order generalized integrators," in *Industrial Electronics, 2008. IECON 2008. 34th Annual Conference of IEEE*, Nov 2008.

[19] M. Villalva, J. Gazoli, and E. Filho, "Comprehensive approach to modeling and simulation of photovoltaic arrays," *Power Electronics, IEEE Transactions on*, vol. 24, no. 5, pp. 1198–1208, May 2009.

[20] K. Hussein, I. Muta, T. Hoshino, and M. Osakada, "Maximum photovoltaic power tracking: an algorithm for rapidly changing atmospheric conditions," *Generation, Transmission and Distribution, IEE Proceedings-*, vol. 142, no. 1, pp. 59–64, Jan 1995.

[21] S. Golestan and J. Guerrero, "Conventional synchronous reference frame phase-locked loop is an adaptive complex filter," *Industrial Electronics, IEEE Transactions on*, vol. 62, no. 3, pp. 1679–1682, March 2015.

[22] P. Rodriguez, R. Teodorescu, I. Candela, A. Timbus, M. Liserre, and F. Blaabjerg, "New positive-sequence voltage detector for grid synchronization of power converters under faulty grid conditions," in *Power Electronics Specialists Conference, 2006. PESC '06. 37th IEEE*, June 2006.